PHYSICAL REVIEW B **92**, 180403(R) (2015)

Electronic structure and spin-orbit driven magnetism in $d^{4.5}$ insulator $Ba_3YIr_2O_9$

S. K. Panda,[1,*] S. Bhowal,[2] Ying Li,[3] S. Ganguly,[2] Roser Valentí,[3] L. Nordström,[4] and I. Dasgupta[1,2,†]

[1]*Centre for Advanced Materials, Indian Association for the Cultivation of Science, Jadavpur, Kolkata-700032, India*

[2]*Department of Solid State Physics, Indian Association for the Cultivation of Science, Jadavpur, Kolkata-700032, India*

[3]*Institut für Theoretische Physik, Goethe-Universität Frankfurt, Max-von-Laue-Strasse 1, 60438 Frankfurt am Main, Germany*

[4]*Department of Physics and Astronomy, Uppsala University, Box 516, SE-75120 Uppsala, Sweden*

(Received 8 September 2015; revised manuscript received 6 October 2015; published 4 November 2015)

We have carried out a detailed first-principles study of a $d^{4.5}$ quaternary iridate $Ba_3YIr_2O_9$ both in its 6H-perovskite-type ambient pressure (AP) phase and also for the high pressure (HP) cubic phase. Our analysis reveals that the AP phase belongs to the intermediate spin-orbit coupling (SOC) regime. This is further supported by the identification of the spin moment as the primary order parameter (POP) obtained from a magnetic multipolar analysis. The large t_{2g} bandwidth renormalizes the strength of SOC and the Ir intersite exchange interaction dominates resulting in long-range magnetic order in the AP phase. In addition to SOC and Hubbard U, strong intradimer coupling is found to be crucial for the realization of the insulating state. At high pressure (HP) the system undergoes a structural transformation to the disordered cubic phase. In sharp contrast to the AP phase, the calculated exchange interactions in the HP phase are found to be much weaker and SOC dominates leading to a quantum spin-orbital liquid (SOL) state.

DOI: 10.1103/PhysRevB.92.180403 PACS number(s): 71.15.Mb, 71.70.Ej, 75.30.Et

The 5*d* Ir based oxide systems have become very fascinating as they offer a ground for understanding the physics driven by the interplay between SOC, on-site Coulomb repulsion (U), crystal-field splitting, and intersite hopping. Many exotic phases like $j_{\text{eff}} = \frac{1}{2}$ Mott state, quantum spin liquid (QSL), topological insulator, and other emergent states have been realized in these systems [1–8]. Kim *et al.* [9,10] first reported spin-orbit driven Mott-insulating state in Sr_2IrO_4, where a large SOC (λ) further splits the t_{2g} orbitals of Ir^{4+} ($5d^5$) into a completely filled $j_{\text{eff}} = \frac{3}{2}$ and a half-filled $j_{\text{eff}} = \frac{1}{2}$ doublet which in the presence of relatively small value of U split into lower and upper Hubbard bands leading to a spin-orbit-driven Mott insulator. In this respect, the 6H perovskite type quaternary iridates $Ba_3MIr_2O_9$, where Ir ions form structural dimers, attracted considerable attention because a nonmagnetic M atom provides a knob to tailor the valence of Ir. Interestingly, Ir in oxidation state other than the usual 4+ (d^5) are not only insulating but also exhibit emergent phases like a spin-orbital liquid (SOL) state in $Ba_3ZnIr_2O_9$ [11] and a pressure induced transition from long-range order to spin liquid state in $Ba_3YIr_2O_9$ [12]. The compound $Ba_3YIr_2O_9$ with fractional charge state $Ir^{4.5+}$ is intriguing on several counts. In the $j_{\text{eff}} = \frac{1}{2}$ picture the insulating state of $Ba_3YIr_2O_9$ is not obvious as Ir with 4.5 electrons is a quarter-filled system as opposed to half-filled d^5 iridates. The origin of pressure induced magnetic transition in this system has also remained unexplored. Furthermore, there could be a possibility of a temperature dependent structural transformation to a charge ordered (CO) state, as seen in $Ba_3NaRu_2O_9$ [13].

Earlier experimental studies on $Ba_3YIr_2O_9$ [14] at ambient pressure (AP) reported a sharp anomaly at 4 K in the heat capacity data although no such feature was seen in the susceptibility data. Later, Dey *et al.* [15] found that the variation of the susceptibility with temperature shows a weak anomaly at about 4 K in agreement with previous heat capacity measurements reflecting the presence of long-range ordering. The susceptibility data [15] follows a Curie-Weiss (CW) behavior with $\theta_{\text{CW}} \sim 0$ and effective moment 0.3 μ_B much less than the spin-only value expected for a $d^{4.5}$ system. On the other hand, the high-pressure (HP) synthesized sample undergoes a structural phase transition and does not order down to 2 K as evidenced from susceptibility, heat capacity, and nuclear magnetic resonance (NMR) measurements and is suggested to be a 5*d*-based, gapless QSL [12].

In view of the above, and also due to the fact that iridates, where Ir ions are in a fractional charge state and form structural dimers, have not been explored before, we have performed density functional theory (DFT) electronic structure calculations within the local density approximation (LDA) as well as LDA + U + SOC that includes the Hubbard U and SOC using the augmented plane waves plus local orbitals (APW + lo) method as implemented in the ELK code [16–18]. The SOC was treated through the second variational method. In this approach, given a value of U using a screened Coulomb potential (Yukawa potential), the corresponding on-site exchange energy J (Hund's coupling) is calculated [17]. The ELK code was also employed to identify the primary order parameter (POP) responsible for breaking of the time reversal (TR) symmetry. Calculations were also done within the generalized gradient approximation (GGA) [19] as well as GGA + U + SOC using the LAPW method as implemented in Wien2k [20] and also projector augmented wave (PAW) method as implemented in the Vienna *ab initio* simulation package (VASP) [21–24]. While these results are very similar to the LDA + U + SOC study, as expected, GGA systematically overestimated the magnitude of the magnetic moment. In order to extract the tight-binding parameters and to understand the crystal field splitting, we have constructed low energy model Hamiltonian using the downfolding procedure as implemented in the Nth order muffin-tin-orbital (NMTO) method [25–27] with self-consistent potentials obtained from linear muffin tin orbital (LMTO) [28] calculations. The technical

*Presently at Uppsala University, Uppsala, Sweden.

†sspid@iacs.res.in

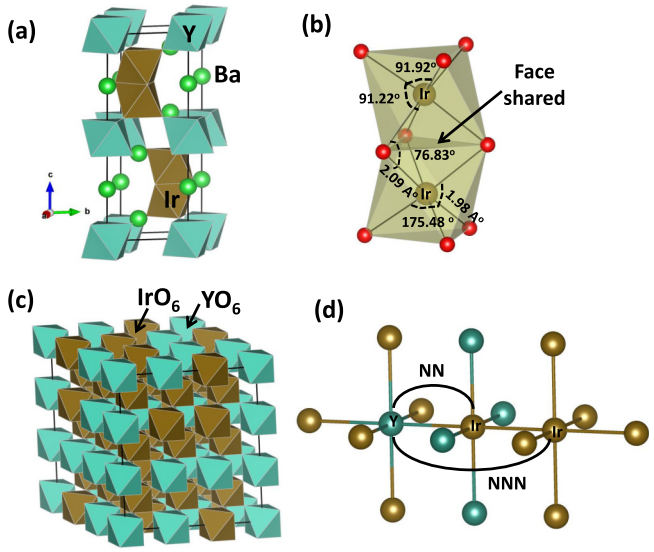

FIG. 1. (Color online) (a) The crystal structure for the hexagonal AP phase of Ba_3YIrO_9. (b) Ir_2O_9 face-shared bioctahedra. (c) Crystal structure for the cubic HP phase $Ba_2Ir(Y_{2/3}Ir_{1/3})O_6$. (d) In the HP phase, the nearest neighbor (NN) of Y is always Ir while the next-nearest neighbor (NNN) of Y can be either Ir or Y due to disorder.

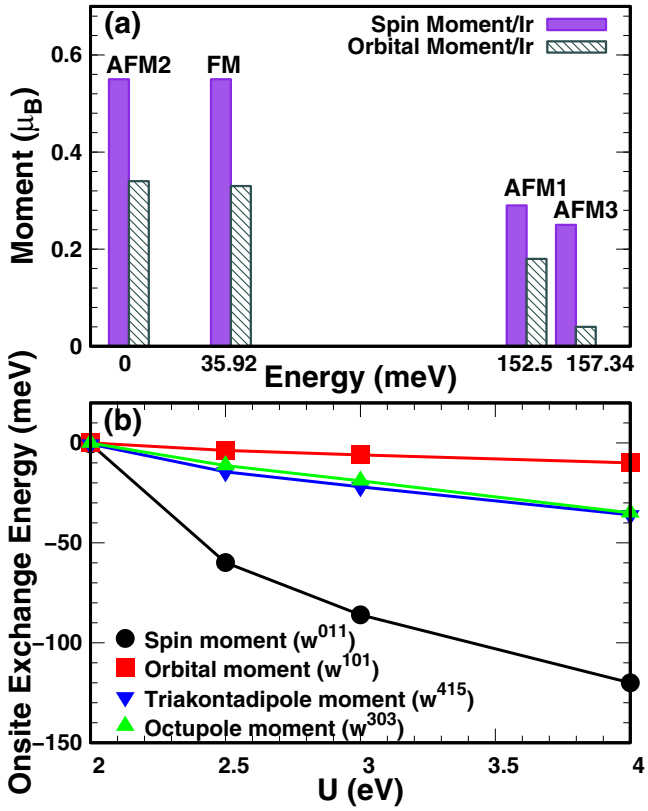

FIG. 2. (Color online) (a) The variation of spin and orbital moment at the Ir site for various magnetic configurations in the AP phase. (b) Variation of on-site exchange energy associated with different order parameters (OP) with the variation of Hubbard U.

details of all the methods are discussed in the Supplemental Materials (SM) [29].

At ambient pressure (AP), $Ba_3YIr_2O_9$ crystallizes in a 6H-perovskite-type structure [12] with space group $P6_3/mmc$ containing two formula units and hence two structural Ir dimers in the unit cell which are connected via O-Y-O paths along the c axis [see Fig. 1(a)]. As shown in Fig. 1(b), each distorted IrO_6 octahedra share their face with the neighboring one, forming Ir_2O_9 face-shared bioctahedra. The high pressure (HP) phase of $Ba_3YIr_2O_9$, on the other hand, crystallizes in the disordered cubic phase $Ba_2Ir(Y_{2/3}Ir_{1/3})O_6$, as shown in Fig. 1(c), where IrO_6 (brown) and YO_6 (cyan) octahedra are arranged, in such a way that each Y has six Ir as its NN but the NNN can be either Y or Ir [see Fig. 1(d)] [12].

We have first investigated the electronic structure of the AP phase of $Ba_3YIr_2O_9$ without any magnetic order. The characteristic feature of the band structure (see Fig. 1 of SM [29]) is the isolated manifold of 12 t_{2g} bands hosting the Fermi level (E_F) arising from the four Ir atoms in the unit cell and is well separated by a gap of 2.5 eV from another complex of eight e_g bands. The t_{2g}-e_g crystal field splitting ($\Delta_{t_{2g}\text{-}e_g}$) is large. The distortion of the IrO_6 octahedron further splits the t_{2g} states into singly degenerate a_1 and doubly degenerate e_1 states with the e_1 states lower in energy by $\Delta_{CF} = 0.16$ eV (see SM for details [29]). The Ba-s and Y-d states are completely empty and hence lie above E_F while O-p states, admixed with Ir-d states, are mostly occupied consistent with the nominal ionic formula $Ba_3^{2+}Y^{3+}Ir_2^{4.5+}O_9^{2-}$ for the system. Due to the small Ir-Ir distance the direct hopping between the a_1 orbital (see SM [29]) is appreciable (−573.9 meV) which is also reflected in the large t_{2g} bandwidth (∼1.88 eV) of $Ba_3YIr_2O_9$.

In order to understand the magnetic properties of the system four different magnetic configurations, namely FM (both the intra- and interdimer couplings are ferromagnetic), AFM1 (both the intra- and interdimer couplings are antiferromagnetic), AFM2 (intradimer coupling is ferromagnetic and interdimer coupling is antiferromagnetic), and AFM3 (intradimer coupling is antiferromagnetic and interdimer coupling is ferromagnetic) have been simulated (see Fig. 2 of SM [29]). The results of our LDA + U + SOC calculation with $U = 4$ eV as obtained using the ELK code are shown in Fig. 2(a). We observe that the AFM2 state has the lowest energy with the spin (orbital) moment on the Ir site to be 0.55 (0.34) μ_B. Spin and orbital moments are in the same direction, as t_{2g} states are more than half filled. The relatively smaller value of $\frac{m_l}{m_s}$ ratio (∼0.62) compared to the other SOC driven $j_{\text{eff}} = 1/2$ iridates, i.e., Sr_2IrO_4 [9], (where it is ∼2) indicates the action of only moderately strong SOC in $Ba_3YIr_2O_9$. Figure 2(a) also reveal that the magnitude of Ir magnetic moments fluctuate for parallel and antiparallel spin configurations in a dimer and only the AFM2 configuration is insulating as illustrated by the plot of band structure and DOS shown in Figs. 3(a) and 3(b), respectively. Although the LDA + U method is less accurate than the LDA method for total energy calculations [30] and has a tendency to favor magnetism because of the additional effective Stoner coupling, it can still be used as a reference for magnetic states as discussed in Ref. [30]. Therefore, a comparison of total energies among various magnetic configurations for $Ba_3YIr_2O_9$ should be reliable in a LDA + U + SOC calculation. The stability of the ferromagnetic (FM) arrangement of Ir atoms in a dimer

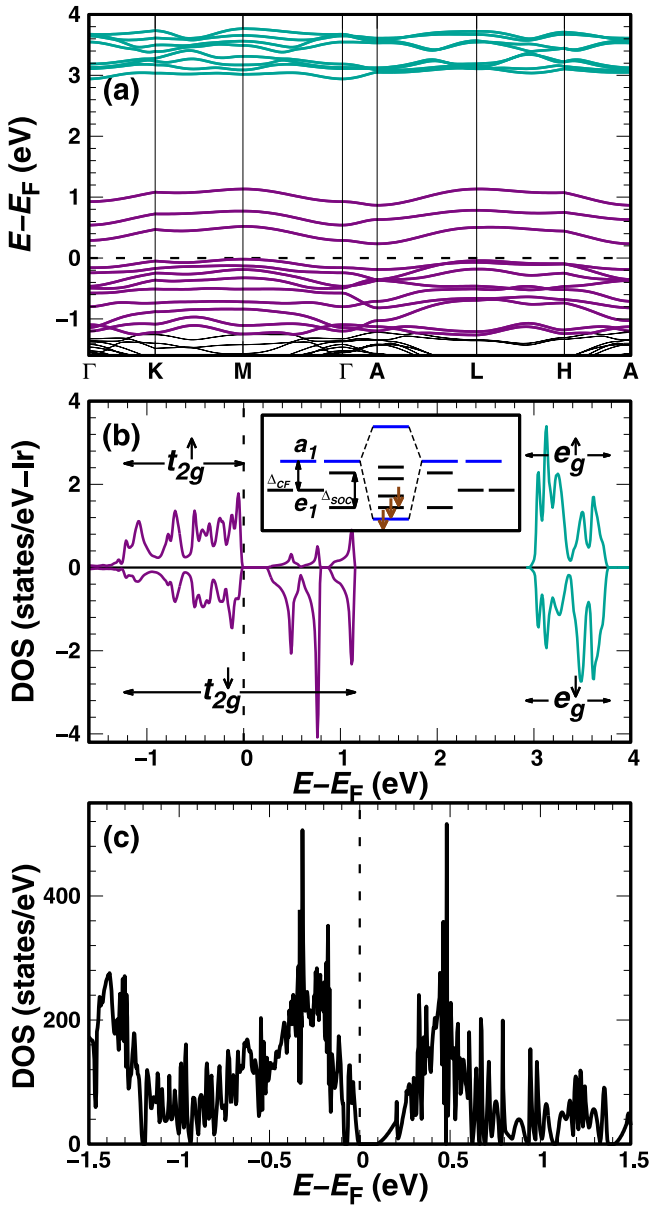

FIG. 3. (Color online) (a) Band structure and (b) partial density of states (DOS) for Ir-d projected onto up and down spin state for the AP phase. The inset shows the schematic diagram to explain the insulating behavior of AP phase. (c) The nonmagnetic DOS for the HP phase of Ba_3YIrO_9 in the presence of SOC and Hubbard U.

in the AFM2 configuration indicates a strong influence of the effective Hund's coupling (J_H) in the system (which is directly related to the on-site exchange parameter J), pointing to the fact that J_H is not only larger than Δ_{CF} but also dominates over the splitting due to SOC (Δ_{SOC}). This hierarchy of energies helps to promote Ir-Ir double exchange. This is in contrast to $Ba_5AlIr_2O_{11}$ [31], where SOC overcomes the Ir-Ir double exchange leading to an AFM arrangement of Ir spins in a dimer.

The origin of the insulating state in $Ba_3YIr_2O_9$ can be explained by the cooperative effect of J_H, Δ_{CF}, Δ_{SOC} and $t_{intradimer}$. In view of comparatively large J_H, we ignore the spin mixing term of the SOC Hamiltonian [32] and only concentrate on the minority t_{2g} bands. This simplification allows us to diagonalize the SOC Hamiltonian, having matrix element $\langle i|\lambda \overline{L}\cdot\overline{S}|j\rangle$ $(i,j=1,2,3)$, and find that the degeneracy of $|1\rangle$ and $|2\rangle$ (i.e., e_1 orbitals) is lifted upon inclusion of SOC, while $|3\rangle$ (a_1 orbital) remains unperturbed [see inset of Fig. 3(b)]. In the presence of strong $t_{intradimer}$ (see Table I of SM [29]), the states will interact strongly with each other and form six nondegenerate states. Three electrons available for a pair of Ir in a dimer in the minority spin channel will lead to an insulating state. Further inclusion of finite Hubbard U (4 eV), which is also crucial to stabilize magnetism, promotes an insulating state with an energy gap of 252 meV as shown in Fig. 3(b). The calculated total magnetic moment in the AFM2 phase is substantially higher from that expected for a quarter-filled $j_{eff}=1/2$ system, indicating the $j_{eff}=1/2$ model may not be relevant here.

The above discussion places $Ba_3YIr_2O_9$ in the intermediate SOC regime and may be attributed to the large t_{2g} bandwidth that substantially renormalizes the strength of the atomic λ. In order to clarify this point further, as well as to identify the order parameter (OP) responsible for breaking the time reversal (TR) symmetry that lead to magnetic order, we have carried out a multipolar (MP) analysis where the rotational invariant local Coulomb interaction is expanded in multipole tensors in the mean field limit. In the present case with Ir-d orbitals the density matrix D ($D=\langle d_n d_n^{\dagger}\rangle$, $d_n^{\dagger}$ and d_n being creation and annihilation vector operators, respectively, for d states of Ir at site n) has 100 independent elements. This information carried by the density matrix can be transformed to expectation values of multipole tensor moments through $w^{kpr}=\mathrm{Tr}\,\Gamma^{kpr}D$, where the multipolar tensor operator Γ^{kpr} is an Hermitian matrix operator as given by Ref. [33] and the indices are determined through the coupling of angular momenta $0\leqslant k\leqslant 2\ell=4$, $0\leqslant p\leqslant 2s=1$, and $|k-p|\leqslant r\leqslant |k+p|$. Altogether there are 18 different multipole tensors (which in total has 100 independent tensor components), of which 9 multipole tensors break the TR symmetry.

In terms of these moments, w^{kpr} the on-site exchange energy for the corresponding state (E_x) can be expanded as [34]

$$E_x=\frac{1}{2}\sum_{kpr}K_{kpr}w^{kpr}w^{kpr}, \qquad (1)$$

where K_{kpr} are the corresponding exchange parameters [17]. Thus the exchange energy (on site) associated with a multipole moment w^{kpr} can be identified [35]. This corresponds to the stabilization of the concerned multipolar order.

The on-site exchange energies corresponding to the TR odd multipole moments in the AFM2 state as a function of U are shown in Fig. 2(b) indicating no change in the hierarchy of the moments with U (see also Table II of SM [29]). From Fig. 2(b) we gather that the spin moment is the POP for the system as it is associated with the highest on-site exchange energy (-120 meV for $U=4$ eV). This is in contrast to the case of SOC driven $j_{eff}=1/2$ Mott insulator Sr_2IrO_4 [36] with a higher order multipole (Triakontadipole) as POP where spin and orbital moments are entangled.

TABLE I. Energy difference between FM and two antiferromagnetic configurations along with the average moment (μ_B/Ir).

Configurations	ΔE/Ir (meV)	Spin (Orb.) moment/Ir
FM	0.0	0.43 (0.14)
AFM-a	−0.41	0.40 (0.16)
AFM-b	−0.24	0.40 (0.16)

Finally to check the possibility of a structural transition accompanied by a CO state, a complete structural relaxation calculation was performed (see SM [29]). Calculations revealed an environment of Ir-Ir dimer to be unaffected ruling out the possibility of a CO state very similar to $Ba_3M^{3+}Ru_2O_9$ systems [37].

Next we have analyzed the HP phase, considering a model structure (see SM [29]), which has been described as a QSL state experimentally. In view of the large size of the unit cell all calculations for the HP phase have been done in the plane wave basis as implemented in the VASP code [21–24]. In Fig. 3(c) we plot the total DOS for the nonmagnetic phase in the presence of SOC and U. We find the system to be an insulator (for $U_{\text{eff}} = U - J = 1.5$ eV) with an energy gap of 87 meV which is in agreement with the experiment [12]. In order to have an estimate of the intersite magnetic interaction in the HP phase, we have considered three magnetic configurations, namely FM, and two antiferromagnetic configurations AFM-a and AFM-b (see SM for description [29]). The results of our calculation are shown in Table I. In sharp contrast to the AP phase the energy difference between the magnetic configurations is small (see Table I), implying the small energy scale of the intersite exchange interaction (J_{ex}) in the HP phase. The AFM configurations being lower in energy, indicate the presence of a weak AFM interaction in the system, consistent with the small value of θ_{CW} ($= -1.6$ K) obtained experimentally [12]. The weak J_{ex} due to disorder prohibits long-range order in the HP phase.

It is quite clear from the above discussion that there is a competition between SOC and J_{ex} in the two phases of $Ba_3YIr_2O_9$. In the AP phase, while J_{ex} wins over SOC so that $\frac{J_{\text{ex}}}{\lambda} > 1$, the HP phase, on the other hand, has much weaker exchange interaction (∼few meV) compared to SOC (for iridates this is typically $\sim 10^2$ meV) making $\frac{J_{ex}}{\lambda} < 1$. The latter condition in the HP phase of $Ba_3YIr_2O_9$ is very similar to the spinel compound $FeSc_2S_4$ [38]. Interestingly the model Hamiltonian considered for $FeSc_2S_4$ is also relevant for the cubic HP phase of $Ba_3YIr_2O_9$ as both of them have quite similar structure, therefore we expect in analogy, the stabilization of SOL state in the HP phase.

In conclusion, our detailed study of electronic and magnetic properties of $Ba_3YIr_2O_9$ both in the AP and HP phase suggest that a competition between J_{ex} and SOC decides the magnetic properties in both phases. In the AP phase the J_{ex} dominates over the SOC leading to long-range magnetic order. The relatively weak value of SOC in the AP phase may be attributed to the large t_{2g} bandwidth in $Ba_3YIr_2O_9$. The identification of the spin moment as the POP, also supports the fact that SOC is not so strong in the AP phase. In the HP cubic phase of $Ba_3YIr_2O_9$ the SOC dominates over the J_{ex} prohibiting long-range order. Finally, we propose the pressure induced modulation of $\frac{J_{\text{ex}}}{\lambda} < 1$ in the HP phase to be responsible for the SOL state.

The authors thank A. V. Mahajan, I. I. Mazin, and S. Streltsov for useful comments. I.D. thanks Department of Science and Technology (DST), Government of India for support. S.B. thanks Council of Scientific and Industrial Research (CSIR), India for a Fellowship. Y.L. and R.V. thank the Deutsche Forschungsgemeinschaft for financial support through grant TR/SFB 49. L.N. thanks Swedish Research Council (VR) for support.

[1] G. Cao, J. Bolivar, S. McCall, J. E. Crow, and R. P. Guertin, Phys. Rev. B **57**, R11039(R) (1998).
[2] R. Arita, J. Kuneš, A. V. Kozhevnikov, A. G. Eguiluz, and M. Imada, Phys. Rev. Lett. **108**, 086403 (2012).
[3] Y. Singh and P. Gegenwart, Phys. Rev. B **82**, 064412 (2010).
[4] M. J. Lawler, A. Paramekanti, Y. B. Kim, and L. Balents, Phys. Rev. Lett. **101**, 197202 (2008).
[5] T. Dey, A. V. Mahajan, P. Khuntia, M. Baenitz, B. Koteswararao, and F. C. Chou, Phys. Rev. B **86**, 140405(R) (2012).
[6] A. Shitade, H. Katsura, J. Kuneš, X.-L. Qi, S.-C. Zhang, and N. Nagaosa, Phys. Rev. Lett. **102**, 256403 (2009).
[7] H.-C. Jiang, Z.-C. Gu, X.-L. Qi, and S. Trebst, Phys. Rev. B **83**, 245104 (2011).
[8] S. K. Panda, S. Bhowal, A. Delin, O. Eriksson, and I. Dasgupta, Phys. Rev. B **89**, 155102 (2014).
[9] B. J. Kim, H. Jin, S. J. Moon, J.-Y. Kim, B.-G. Park, C. S. Leem, J. Yu, T. W. Noh, C. Kim, S.-J. Oh, J.-H. Park, V. Durairaj, G. Cao, and E. Rotenberg, Phys. Rev. Lett. **101**, 076402 (2008).
[10] B. J. Kim, H. Ohsumi, T. Komesu, S. Sakai, T. Morita, H. Takagi, and T. Arima, Science **323**, 1329 (2009).
[11] A. Nag *et al.*, arXiv:1506.04312.
[12] T. Dey, A. V. Mahajan, R. Kumar, B. Koteswararao, F. C. Chou, A. A. Omrani, and H. M. Ronnow, Phys. Rev. B **88**, 134425 (2013).
[13] S. A. J. Kimber, M. S. Senn, S. Fratini, H. Wu, A. H. Hill, P. Manuel, J. P. Attfield, D. N. Argyriou, and P. F. Henry, Phys. Rev. Lett. **108**, 217205 (2012).
[14] Y. Doi and Y. Hinatsu, J. Phys.: Condens. Matter **16**, 2849 (2004).
[15] T. Dey, R. Kumar, A. V. Mahajan, S. D. Kaushik, and V. Siruguri, Phys. Rev. B **89**, 205101 (2014).
[16] D. Singh and L. Nordström, *Planewaves, Pseudopotentials, and the LAPW method* (Springer, New York, 2006).
[17] F. Bultmark, F. Cricchio, O. Grånäs, and L. Nordström, Phys. Rev. B **80**, 035121 (2009).
[18] ELK is available at http://elk.sourceforge.net.

[19] J. P. Perdew, K. Burke, and M. Ernzerhof, Phys. Rev. Lett. **77**, 3865 (1996).

[20] P. Blaha, K. Schwarz, G. K. H. Madsen, D. Kvasnicka, and J. Luitz, WIEN2k, *An Augmented Plane Wave + Local Orbitals Program for Calculating Crystal Properties* (Karlheinz Schwarz, Techn. Universiat Wien, Austria, 2001).

[21] P. E. Blöchl, Phys. Rev. B **50**, 17953 (1994).

[22] G. Kresse and D. Joubert, Phys. Rev. B **59**, 1758 (1999).

[23] G. Kresse and J. Hafner, Phys. Rev. B **47**, 558(R) (1993).

[24] G. Kresse and J. Furthmüller, Phys. Rev. B **54**, 11169 (1996).

[25] O. K. Andersen and T. Saha-Dasgupta, Phys. Rev. B **62**, R16219(R) (2000).

[26] O. K. Andersen, T. Saha-Dasgupta, R. W. Tank, C. Arcangeli, O. Jepsen, and G. Krier, in *Electronic Structure and Physical Properties of Solids. The Uses of the LMTO Method*, Springer Lecture Notes in Physics (Springer, Berlin, 2000), p. 3.

[27] O. K. Andersen, T. Saha-Dasgupta, and S. Ezhov, Bull. Mater. Sci. **26**, 19 (2003).

[28] O. K. Andersen and O. Jepsen, Phys. Rev. Lett. **53**, 2571 (1984).

[29] See Supplemental Material at http://link.aps.org/supplemental/10.1103/PhysRevB.92.180403 for theoretical techniques.

[30] A. G. Petukhov, I. I. Mazin, L. Chioncel, and A. I. Lichtenstein, Phys. Rev. B **67**, 153106 (2003).

[31] S. V. Streltsov, J. Terzic, J. C. Wang, F. Ye, D. I. Khomskii, W. H. Song, S. J. Yuan, S. Aswartham, and G. Cao, arXiv:1505.00877.

[32] S. Sarkar, M. De Raychaudhury, I. Dasgupta, and T. Saha-Dasgupta, Phys. Rev. B **80**, 201101(R) (2009).

[33] F. Cricchio, O. Grånäs, and L. Nordström, Eur. Phys. Lett. **94**, 57009 (2011).

[34] F. Cricchio, F. Bultmark, and L. Nordström, Phys. Rev. B **78**, 100404(R) (2008).

[35] F. Cricchio, F. Bultmark, O. Grånäs, and L. Nordström, Phys. Rev. Lett. **103**, 107202 (2009).

[36] S. Ganguly, O. Grånäs, and L. Nordström, Phys. Rev. B **91**, 020404(R) (2015).

[37] M. S. Senn, S. A. J. Kimber, A. M. Arevalo Lopez, A. H. Hill, and J. P. Attfield, Phys. Rev. B **87**, 134402 (2013).

[38] G. Chen, L. Balents, and A. P. Schnyder, Phys. Rev. Lett. **102**, 096406 (2009); G. Chen, A. P. Schnyder, and L. Balents, Phys. Rev. B **80**, 224409 (2009); S. Sarkar, T. Maitra, R. Valentí, and T. Saha-Dasgupta, *ibid.* **82**, 041105(R) (2010).